Journal of Chemical and Pharmaceutical Sciences -JCHPS (2025) 18 (3): 33-43
Online ISSN: Online 2349-8552, Print ISSN: 0974-2115
Research Article | Chemical Sciences | MCI Approved | Peer-Reviewed | Referred | OA Journal |

Spectral, Microscopic and Anticancer Activity Investigation on Dimethyl Yellow/Cyclodextrin Doped ZnO Nanocomposites

Palanichamy Ramasamy[1], Ayyadurai Mani[2], Poomalai Senthilraja[3], Narayanasamy Rajendiran[1,*]
[1] Department of Chemistry, Annamalai University, Annamalai Nagar, India
[2] Centre for Advanced Energy Materials, SRM TRP Engineering College, Tiruchy, India
[3] Department of Bioinformatics, Bharathidasan University, Tiruchy, India.

Received: 25 April 2025 / Accepted: 26 May 2025/ Published online: 01 Jul 2025
*Corresponding Author Email: drrajendiran@rediffmail.com

ABSTRACT

The study investigates nanocomposites formed by combining dimethyl yellow (DMY) with cyclodextrin-ZnO nano. Various analytical techniques were employed to characterize these materials. DMY exhibited single emission in different solvents, α-CD and β-CD environments. When comparing the emissions in water, a red shift occurred in DMY with α-CD and β-CD, the emission peaks becoming more defined. The flat band distance of DMY is higher than the CD cavity sizes, hence the DMY could only achieve partial encapsulation. The interaction between DMY and β-CD proved firmer than α-CD. When examining the ZnO/DMY/β-CD nanocomposites, both red and blue shifts were detected in absorption and fluorescence measurements relative to the DMY/CD. XRD results indicated that the nanoparticle size is 17 nm, while TEM-EDS analysis showed 24 nm particles. TEM imaging revealed that the ZnO/DMY/β-CD formed nanocrystal. Additionally, the study explored DMY's potential anticancer properties through molecular docking analyses.

KEY WORDS:

Dimethyl yellow, Zinc oxide nano, Cyclodextrin, Molecular docking, Anticancer.

1. Introduction

Zinc oxide nanoparticles (ZnO NPs) are emerging as a promising and economical nanomaterial with low toxicity. Their versatility has attracted considerable interest for various biomedical applications, such as cancer therapy, bacterial inhibition, reducing oxidative stress, managing diabetes, and alleviating inflammation [1,2]. Additionally, they are utilized in drug delivery systems and biomedical imaging. A significant advantage of ZnO nanoparticles measuring under 100 nm is their biocompatibility, making them particularly advantageous for medical applications and research advancements.

Historically, cancer treatments have relied on chemotherapy, radiation therapy, and surgical procedures. While these methods can effectively eradicate cancer cells, their non-selective nature often leads to severe side effects. The advent of nanomedicine presents a potential remedy to these challenges [3-5]. Treatments based on nanomaterials offer several benefits: they exhibit excellent biocompatibility, can be easily modified, specifically target cancer cells, and efficiently deliver therapeutic agents. The essential role of zinc ions as a nutrient, coupled with the biodegradable nature of ZnO nanomaterials, positions them as a promising therapeutic platform for cancer treatment [4-9].

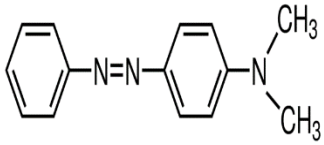

Figure 1. Structure of dimethyl yellow [DMY]; methyl yellow or 4-dimethyl amino azobenzene C.I. 11020, is an organic compound with the formula $C_{14}H_{15}N_3$. It is an azo dye derived from dimethylaniline. It is a yellow solid.

Journal of Chemical and Pharmaceutical Sciences -JCHPS (2025) 18 (3): 33-43
Online ISSN: Online 2349-8552, Print ISSN: 0974-2115
Research Article | Chemical Sciences | MCI Approved | Peer-Reviewed | Referred | OA Journal |

Dimethyl yellow (4-dimethyl amino azobenzene, DMY, Figure 1) is primarily used as a dye, particularly in the past for coloring waxes and polishes, but is now largely considered a carcinogen due to its potential to induce liver cancer in animals, making its use highly restricted; it is also sometimes used in research as a positive control for cancer studies. Due to the importance of Zno nano and DMY, the present research project aims to achieve three primary objectives: a) synthesize and analyze DMY/CD-doped ZnO nanocomposites, b) determine the structural characteristics of the synthesized nanomaterials, c) assess the anticancer properties of DMY.

2. Experimental

2.1. Drug/CD inclusion complex preparation

Varying concentrations of α-CD or β-CD (0.1 to 1.0×10^{-2} M) were prepared in 10 ml volumetric flasks. In each flask added 0.2 ml of DMY stock solution (2×10-2 M), followed by dilution with triple-distilled water to the 10 ml mark. The solutions were thoroughly mixed, yielding a consistent DMY concentration of 4×10^{-4} M across all samples. All measurements were performed at 298 K.

2.2. Computational PM3 Studies

Spartan 08 software used to analyze the ground state molecular geometries of DMY, CD, and their inclusion complexes. They constructed two different orientations of inclusion complexes and evaluated them by PM3 method in gas phase conditions with Gaussian 09W software. This analysis helped determine which configuration yielded the most energetically favorable complexation energy.

2.3. ZnO and DMY/CD Doped ZnO Nanocomposites Preparation

ZnO nanoparticles were synthesized by first dissolving 0.01 M zinc sulphate in 100 ml deionized water and heating the solution to 50-60°C for 20-30 minutes. A reaction mixture was created by combining $ZnSO_4$ and NaOH solutions in a 1:1 molar ratio, which was stirred at 300 K for 12 hours. The white ZnO precipitate was collected via centrifugation, washed multiple times, and dried in an oven at 100°C for 6 hours [10–14]. Subsequent analysis showed that the synthesized ZnO nanoparticles measured between 25 and 50 nanometers in size.

To prepare the nanocomposite, DMY (2×10^{-3} M) was dissolved in 20 ml of ethanol and slowly added to an aqueous CD solution (1×10^{-2} M in 80 ml). This DMY/CD inclusion complex was combined with zinc sulphate solution (0.01 M in 100 ml) and heated to 50°C on a magnetic stirrer hot plate for one hour. 1 % sodium hydroxide was added dropwise with vigorous stirring, which continued for 1-2 hours. The solution was then freeze-dried at -80°C under vacuum using a mini-lyophilizer. The resulting powder, identified as ZnO/DMY/CD nanocomposite, was collected for further analytical studies.

2.4. Molecular Docking Method

Auto Dock software package that employs multiple computational approaches including simulated annealing, local gradient searches, and genetic algorithms [15,16]. Auto Dock 4.2.6 and Auto Dock Vina software were used [17-22]. The docking simulations utilize the Lamarckian genetic algorithm alongside the Solis & Wets local search method. Initial molecular configurations are randomly assigned. Each simulation comprises 10 distinct runs, each limited to 25 x 10^4 energy evaluations, with a population size of 150. The search parameters include a 0.2 Å translational step, with quaternion and torsion steps set at 5.

Journal of Chemical and Pharmaceutical Sciences -JCHPS (2025) 18 (3): 33-43
Online ISSN: Online 2349-8552, Print ISSN: 0974-2115
Research Article | Chemical Sciences | MCI Approved | Peer-Reviewed | Referred | OA Journal |

3. Result and Discussion

3.1. Effect of cyclodextrins and solvents on DMY

Absorption analysis of dimethyl yellow (DMY), revealed consistent peaks at 415 and 266 nm in water, α-CD and β-CD solutions (Table 1, Figure 2). Increasing cyclodextrin concentration led to a slight increase in absorbance at these wavelengths but did not significantly alter the spectral maxima. DMY exhibited a single fluorescence emission peak (470 nm) in all three environments. Upon growing the α-CD or β-CD concentrations, the emission maximum red-shifted to 535 nm, and the emission intensity increased steadily. These changes suggest that DMY was successfully encapsulated within the CD cavity. The emission spectra became sharper in the CD solutions compared to water, likely due to the non-polar environment and restricted rotational movement of DMY within the CD cavities. Similar spectral changes indicate that both α-CD and β-CD form similar inclusion complex. The plots $1/(A-A_0)$ vs $1/[CD]$ and $1/(I-I_0)$ vs $1/[CD]$ and the presence of an isosbestic point in the absorption spectrum indicated the formation of 1:1 inclusion complex. The binding energy (K $x10^5$ M^{-1}) (DMY/α-CD: abs-125, flu-155, DMY/β-CD: abs-121, flu:501) and negative Gibbs free energy values demonstrated that the binding process occurred spontaneously and achieved thermodynamic stability under the experimental conditions.

Table 1: Absorption and fluorescence spectral maxima of DMY with different solvents, α-CD and β-CD. The absorption maxima of DMY appears in cyclohexane to ethanol is 408, 253 nm, while in water and CD red shift is noticed around 415, 266 nm. The emission maximum appears from 470 to 535 nm.

Solvents	λ_{abs}	log ε	λ_{flu}
Cyclohexane	408 253	3.31 3.02	500
1,4-Dioxane	408 253	3.36 2.97	480
Ethyl acetate	408 250	3.58 3.19	500
Acetonitrile	408 260	3.41 2.96	510
2-Propanol	408 256	3.52 3.14	500
Ethanol	408 255	3.48 3.06	507
Water	415 266	3.15 3.04	470
α-CD [0.01 M]	416 267	3.23 3.24	535
β-CD [0.01 M]	417 267	3.24 3.24	535
α-CD K (1:1) $x10^5$ M^{-1}	125	-	155
β-CD K (1:1) $x10^5$ M^{-1}	121	-	501
α-CD ΔG (kcalmol^{-1})	-11.9	-	-12.7
β-CD ΔG (kcalmol^{-1})	-11.7	-	-15.7
Excitation wavelength (nm)	-	-	360

Journal of Chemical and Pharmaceutical Sciences -JCHPS (2025) 18 (3): 33-43
Online ISSN: Online 2349-8552, Print ISSN: 0974-2115
Research Article | Chemical Sciences | MCI Approved | Peer-Reviewed | Referred | OA Journal |

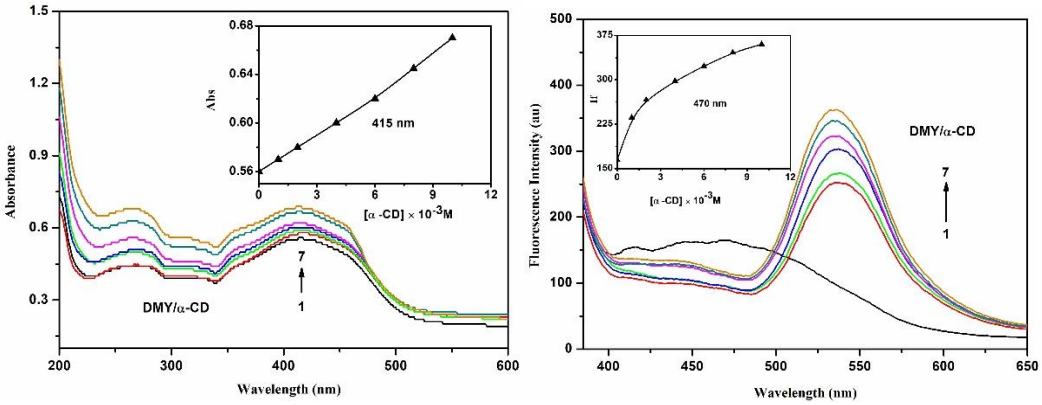

Figure 2: Absorption and fluorescence spectra of DMY in different α-CD concentrations (M): (1) 0, (2) 0.001, (3) 0.002, (4) 0.004, (5) 0.006, (6) 0.008, (7) 0.01. Insert figure: Absorbance/I_F *vs* [α-CD]. Upon increasing the α-CD concentrations, the absorption and spectral maxima of DMY was appearing at 415, 266 nm in water, α-CD are given; while the emission maximum red shifted (470 to 535 nm) and the absorbance and emission intensity regularly increased (insert Fig).

To investigate the inclusion complexation process, DMY's absorption and emission spectra were analyzed with varying polarity of the solvents (Table 1). DMY consistently showed two absorption peaks in all solvents, similar to observations in 4-aminoazobenzene (4AAB) and azobenzene (AB) [23-28]. DMY's absorption maxima (λ_{abs}~ 415, 216 nm) exhibited a greater red shift compared to AB (λ_{abs}~ 317 nm, λ_{emi}~ 362 nm) and 4AAB (λ_{abs}~ 380 nm, λ_{emi}~ 430 nm). DMY displayed a single emission peak in all the solvents, and the absorption and emission maxima showing red shifts from non-polar to polar solvents. Notably, water produced broader absorption and emission spectral wavelengths than other solvents. The different spectral shifts observed between regular solvents and CD solution suggest successful encapsulation of DMY within the CD cavity [29-25]. The enhanced electronic delocalization effect from these groups to the aromatic ring explains the considerable red shift observed in DMY and 4AAB compared to AB. The observed red or blue shifts in the ground and first excited states reflect increased delocalization between the azo and the dimethyl amino groups and the conjugated double bands [23-35].

3.2. Molecular Modeling

The ground state geometries of DMY, α-CD, β-CD, and DMY/CD were optimized using the PM3 method. Table 2 documents the HOMO, LUMO (Figure 3), and various thermodynamic property values for all components. When DMY entered the CD cavity, significant changes in these parameters were observed between the guest, host and the inclusion complexes. The DMY/β-CD inclusion complex showed more negative ΔE, ΔH and ΔG than that of DMY/α-CD indicates spontaneous and exothermic formation. The negative entropy (ΔS) due to the disorder of the system.

The optimization process was conducted by two ways: Type I (C_6H_5-N=N- group) and Type II ($(CH_3)_2$N- group) of the DMY molecule encapsulated in the CD cavity. The internal diameters of α-CD and β-CD are approximately 5.6 and 6.5 Å respectively; both CD having a height of 7.8 Å. DMY's horizontal band length (10.63 Å) exceeds the dimensions of both CD cavities, suggest DMY partially entered (either the aromatic ring or dimethyl amino group) in the CD cavity. Further, formation of the hydrogen banding between the hydroxyl groups on the primary and secondary rims of different CD molecules stabilized the complexes, hence the absorption and emission intensities of DMY in CD is varied from the solvents.

Journal of Chemical and Pharmaceutical Sciences -JCHPS (2025) 18 (3): 33-43
Online ISSN: Online 2349-8552, Print ISSN: 0974-2115
Research Article | Chemical Sciences | MCI Approved | Peer-Reviewed | Referred | OA Journal |

Table 2: Energetic features, thermodynamic parameters and HOMO-LUMO energy calculations for DMY and its inclusion complexes by semiempirical PM3 method. The HOMO-LUMO, dipole, internal energy, free energy, enthalpy, and entropy values of free DMY, CD and the inclusion complexes are given.

Properties	DMY	α-CD	β-CD	DMY/α-CD	DMY/β-CD
E_{HOMO} (eV)	-8.44	-10.37	-10.35	-8.38	-8.49
E_{LUMO} (eV)	-0.71	1.26	1.23	-0.83	-0.86
$E_{HOMO} - E_{LUMO}$ (eV)	7.73	-11.63	-11.58	7.54	7.62
Dipole (D)	1.55	11.34	12.29	10.04	10.71
E (kcal mol^{-1})	-86.66	-1247.62	-1457.63	-1172.81	-1379.85
ΔE (kcal mol^{-1})	-	-	-	-11.85	-8.88
G (kcal mol^{-1})	-134.58	-676.37	-789.52	-853.09	-965.54
ΔG (kcal mol^{-1})	-	-	-	-42.14	-41.44
H (kcal mol^{-1})	-174.14	-570.84f	-667.55	-724.30	-819.85
ΔH (kcal mol^{-1})	-	-	-	-20.68	-22.44
S (kcal/mol-Kelvin)	0.132	0.353	0.409	0.431	0.490
ΔS (kcal/mol-Kelvin)	-	-	-	0.054	0.055
ZPE	163.76	635.09	740.56	801.14	906.08

kcal/mol; **kcal/mol-Kelvin; ZPE = Zero-point vibration energy

Figure 3 illustrate considerable variations in HOMO-LUMO energy across all both the inclusion complexes. In these illustrations, nitrogen atoms appear blue, while green and red colors in HOMO-LUMO represent -ve and +ve phases. In the molecular electrostatic potential (MEP) figures, the red regions indicate that atoms with greater electronegative charge. The larger (E_{HOMO}-E_{LUMO}) values correlate with higher stability. The isolated DMY molecule demonstrated lower stability than its inclusion complexes, with the DMY/β-CD inclusion complex showing a more negative HOMO-LUMO gap, confirming its greater stability compared to DMY/α-CD complexes [23-35].

3.3. Effect of DMY/β-CD Doping on ZnO nano

The absorption and emission spectra of ZnO, ZnO/DMY, ZnO/β-CD, and DMY/β-CD doped ZnO nanocomposites in solution phase are measured. Pure ZnO nanoparticles appearing as a white precipitate exhibited absorption at 320 nm and emission at 420 and 355 nm. It is known that, absorption and emission behaviours are influenced by the particle size, shape, metallic composition, and environmental factors, with intensity not directly proportional to particle quantity [10-14]. When DMY doped on the ZnO nanoparticle, the absorption and the emission maxima shifted to 353 and 465 nm respectively. After β-CD doped on ZnO nanoparticles, the ground and excited state maxima moved to 250 nm and 398 nm respectively. When DMY/β-CD doped on ZnO nanoparticles, the S_0 and the S_1 state maxima red-shifted to 430, 255 nm, and 510 nm respectively. These spectral shifts (both red and blue) provide evidence that DMY/CD successfully doped the ZnO nanoparticles. Generally, successful doping of nanoparticles by other molecules is characterized by changes in spectral intensity and variations in spectral profiles.

3.4 FE-SEM and TEM images

The morphology and composition of ZnO nano, DMY, ZnO/β-CD, and ZnO/DMY/β-CD nanocomposites were characterized using FE-SEM and EDAX techniques (Figure 4). ZnO particles appeared as small clustered balls; ZnO/β-CD exhibited a sheet-like morphology; DMY displayed a micro-rod shape, while ZnO/DMY/β-CD presented a distinctive coral-shaped structure. FE-SEM-EDAX analysis provided elemental composition data: (a) ZnO nanoparticles: zinc~57.34% and oxygen~ 42.66%; (b) ZnO/β-CD nano: zinc~19.67%, oxygen~54.42%, and carbon~25.91%; (c) DMY: carbon~79.20% and nitrogen~20.80 %; and (d) ZnO/DMY/β-CD nano: zin~ 23.0%, carbon~ 20.94%, oxygen~51.54%, and nitrogen~ 4.22%. The differences observed in FE-SEM morphologies and atomic

Journal of Chemical and Pharmaceutical Sciences -JCHPS (2025) 18 (3): 33-43
Online ISSN: Online 2349-8552, Print ISSN: 0974-2115
Research Article | Chemical Sciences | MCI Approved | Peer-Reviewed | Referred | OA Journal |

compositions between ZnO nano, DMY, and the ZnO/DMY/β-CD composite confirm the successful formation of novel nanocomposite structures.

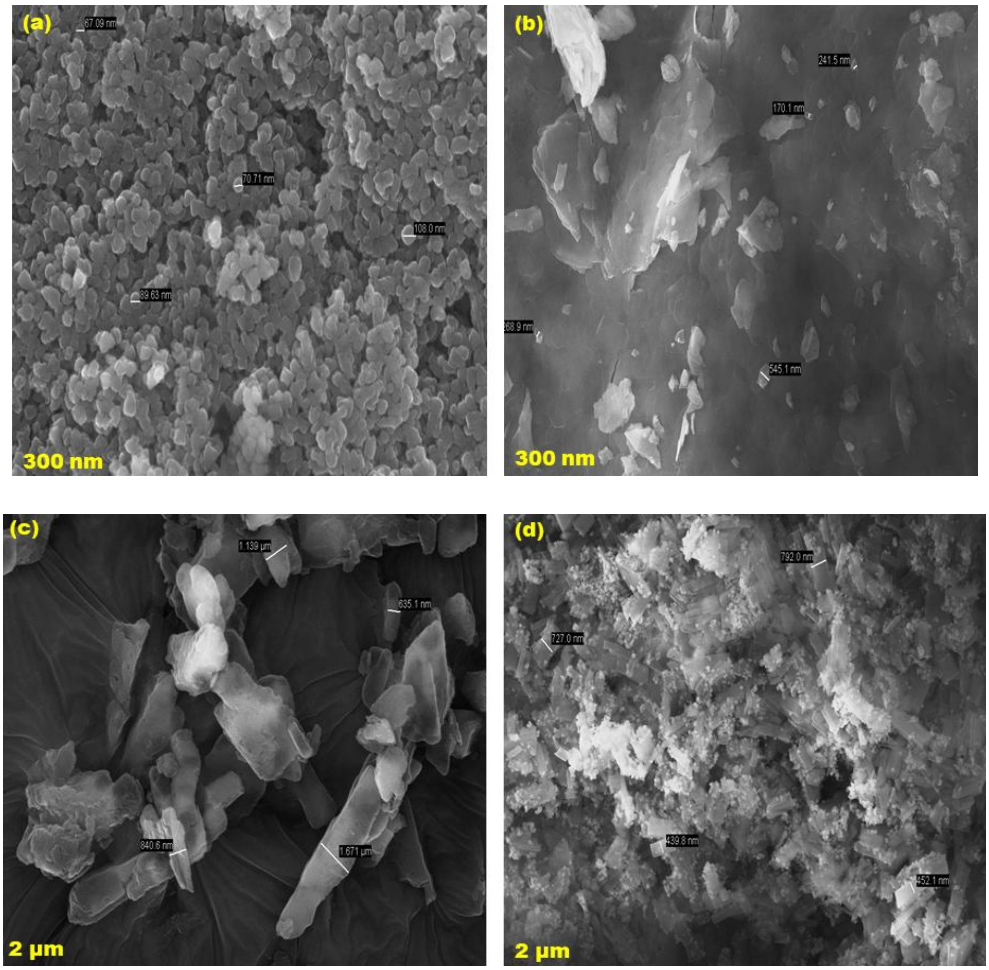

Figure 4: FE-SEM images for (a) ZnO, (b) ZnO/β-CD, (c) DMY, (d) ZnO/DMY/β-CD inclusion complexes.

TEM images of ZnO, ZnO/β-CD and ZnO/DMY/β-CD are displayed in Figure 5. Nano sheet like structures found in the ZnO nanomaterials while nanorod like structure is formed in ZnO/β-CD. TEM image of ZnO nanosheet were seen to uniformly spherical particles between 20 and 44 nm size and in ZnO/β-CD nano, the particles size between 20 and 40 nm. ZnO/DMY/β-CD nanorod size were displayed to be between 20-33 nm. The TEM-EDX data supported the formation of nanoparticles: (a) ZnO nano: 69.84 % of zinc and 30.16 % of oxygen, (b) ZnO/β-CD nano: zinc~ 8.79 %, oxygen~ 44.59 % and carbon~ 46.61 %, (c)) ZnO/DMY/β-CD nano: zinc~ 22.10 %, carbon ~42.70 %, oxygen~ 32.22 % and nitrogen~ 2.99 %. The presence of DMY/β-CD doped ZnO is confirmed by the EDX data.

The nanoparticles size is measured by X-RD and HR TEM methods. In HR-TEM, IMAGE-J software was used and the average particle size calculated by Origin software. The particle size is given below: ZnO nano – 24.98 nm, ZnO/β-CD – 23.98 nm, ZnO/DMY/β-CD Nano – 24.03 nm. In XRD method, the particle size is measured by Scherer equation [$D = K\lambda/\beta Cos\theta$], D = Average particle size, K = constant value (0.94): The particle size is given below: ZnO nano – 19.30 nm, β-CD– 23.84, DMY- 24.07 nm, ZnO/β-CD- 20.69 nm, and ZnO/DMY/β-CD Nano– 17.77 nm. Compared to XRD method, 4-7 nm particle size is varied in HR-TEM method.

Journal of Chemical and Pharmaceutical Sciences -JCHPS (2025) 18 (3): 33-43
Online ISSN: Online 2349-8552, Print ISSN: 0974-2115
Research Article | Chemical Sciences | MCI Approved | Peer-Reviewed | Referred | OA Journal |

3.5 Powder X-Ray Diffractogram

The ZnO diffraction peaks were compared and confirmed by JCPDS: 03-065-3411 data and the JCPDS card number is 800-075. The diffraction peaks of the ZnO confirmed by the presence of hexagonal structure which is corresponds to hkl planes at (100), (002), (101), (102), (103), (110), (112), and (201). The ZnO nanoparticles showed eight diffraction peaks at 31.80°, 34.51°, 36.21°, 47.52°, 56.61°, 62.90°, 67.91°, 69.92° and the β-CD exhibited eight peaks at 13.39°, 19.93°, 23.50°, 27.65°, 31.96°, 35.54°, 40.58°, 48.90°. The ZnO/β-CD displayed ten peaks at 10.15°, 15.18°, 25.41°, 28.38°, 34.92°, 42.29°, 49.77°, 59.16°, 63.32°, 70.33° and DMY showed six peaks at 13.01°, 15.16°, 17.87°, 20.95°, 22.31°, 26.47°. ZnO/DMY/β-CD nano exhibited ten peaks at 10.45°, 12.21°, 25.14°, 28.24°, 32.82°, 34.85°, 41.85°, 51.02°, 58.56°, 62.90°. Compared to DMY, the ZnO/DMY/β-CD nanomaterials showed different patterns and peak intensities providing evidence for the formation of nanomaterials. The appearance of numerous prominent peaks across the 10–80-degree range further supported the formation of ZnO/DMY/β-CD nanomaterials.

3.6 Infrared Spectral Studies

FTIR spectral analysis of ZnO nano, DMY, ZnO/DMY, ZnO/β-CD, and ZnO/DMY/β-CD are analysed. The ZnO nanoparticles showed IR frequencies at 3325, 1587, 1450, 592, and 513 cm^{-1}, resulting from the Zn^{+2} ion to ZnO nano. The 3325 cm^{-1} wavenumber confirms the presence of ZnO, while the peaks at 592 and 513 cm^{-1} indicate the presence of ZnO nanoparticles. Previous research has reported that pure ZnO nanoparticles show a characteristic IR peak for ZnO band at 595 cm^{-1}, while the broad band at 3507 cm^{-1} corresponds to O-H group absorption.

When β-CD was doped to ZnO nano, significant changes were noted in the frequency: 3325 cm^{-1} shifted to 3280 cm^{-1}, 1587 and 1450 cm^{-1} moved to 1614 and 1514 cm^{-1}, and 592 and 513 cm^{-1} peaks shifted to 594 and 526 cm^{-1}. These spectral differences suggest CD covered the ZnO nanoparticles. The DMY FTIR spectrum revealed several characteristic peaks: azo group stretching at 1359 cm^{-1}, phenyl ring CH stretching at 2900 cm^{-1}, aromatic ring stretching at 1615 and 1516 cm^{-1}, out-of-plane bending frequencies at 939 and 812 cm^{-1}, C-N-C bending at 532 cm^{-1}, C-NH_3 vibration at 2810 cm^{-1}, and CH out-of-plane bending at 765 and 727 cm^{-1}.

In the ZnO/DMY/β-CD nanocomposite, these frequencies exhibited notable shifts: the azo group stretching shifted from 1359 to 1357 cm^{-1}, phenyl ring CH stretching from 2900 to 2924 cm^{-1}, aromatic ring stretching from 1615 and 1516 cm^{-1} to 1620 and 1497 cm^{-1}, out-of-plane bending from 939 and 812 cm-1 to 941 and 815 cm^{-1}, and C-N-C bending from 532 cm^{-1} to 1615 and 538 cm^{-1}. The C-NH_3 frequency at 2810 cm^{-1} disappeared, while CH out-of-plane bending frequencies shifted from 765 and 727 cm^{-1} to 754 and 696 cm^{-1}. The significant frequency changes observed in ZnO/DMY/β-CD nanocomposites compared to DMY and ZnO/β-CD provide strong evidence that DMY/β-CD successfully doped the ZnO nanoparticles.

3.7 Differential Thermal Analysis

The DTA profiles for pure ZnO nanoparticles, DMY, ZnO/β-CD, and ZnO/DMY/β-CD are measured. In ZnO nanoparticles, two exothermic and three endothermic peaks at 226.1, 546.7 °C, and 272.6, 731.1, 919.2 °C were observed, respectively. DMY displayed two exothermic and one endothermic peak at 334.8, 676.1 °C, and 114.5 °C, respectively. In β-CD, one exothermic peak (128.6 °C) was noted. In the ZnO/β-CD nano, two exothermic and four endothermic peaks (224.3, 932.4 °C, and 265.2, 354.6, 749.8, 884.1°C were detected. The ZnO/DMY/β-CD nanocomposite exhibited two endothermic and three exothermic peaks (370.2, 972.5 °C, and 250.3, 705.8, 1007.8 °C), respectively. The endothermic peaks in the nanomaterials are attributed to the release of water from the cyclodextrins (CDs). Notably, a new peak appears in the ZnO/DMY/β-CD composite that confirms the formation of the nanomaterials, differing from those observed in pure DMY and ZnO.

Journal of Chemical and Pharmaceutical Sciences -JCHPS (2025) 18 (3): 33-43
Online ISSN: Online 2349-8552, Print ISSN: 0974-2115
Research Article | Chemical Sciences | MCI Approved | Peer-Reviewed | Referred | OA Journal |

3.8 Molecular Docking

Molecular docking analysis was conducted by Dassault Systems BIOVIA Discovery Studio v22.1.100 (licensed version). The 3D structure of the target protein (Epidermal Growth Factor Receptor (EGFR) complexed with epiregulin (EREG)) was obtained from the Protein Data Bank (PDB ID:5WB7). The protein preparation involved removing water molecules and ions, as well as adding hydrogen atoms. Following the grid setup, docking was performed to identify optimal binding positions [15-21].

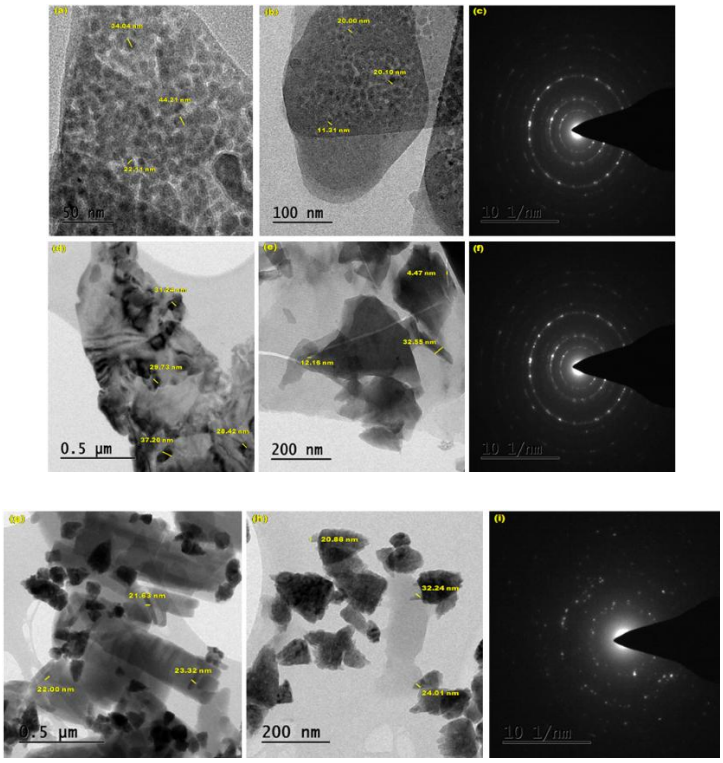

Figure 5: HR-TEM images for (a-c) ZnO, (d-f) ZnO/β-CD, (g-i) ZnO/DMY/β-CD.

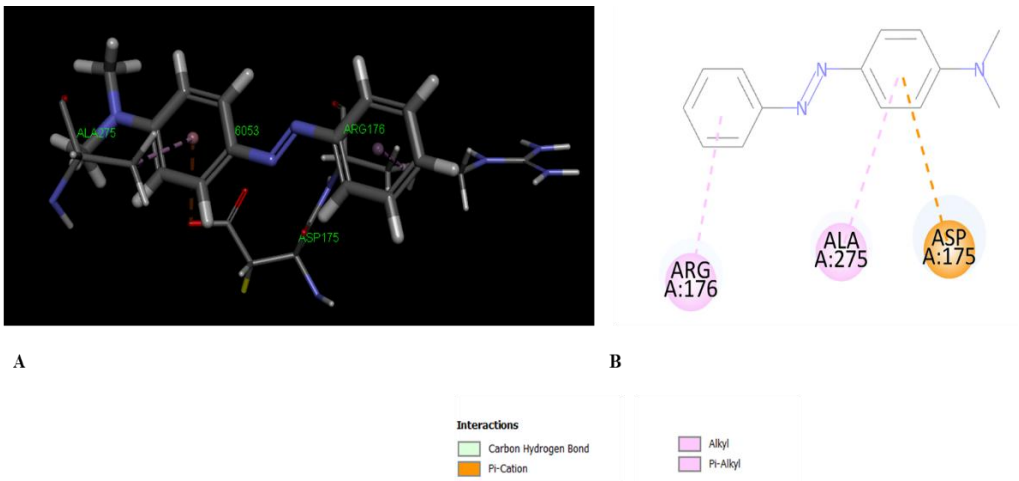

Figure 6: Anticancer activity of DMY **(ID No. 6053)** with 1r51 amino acid residues. DMY interacting with 1r51 protein the amino acid residues- two C-H interaction noticed in alkyl at Arg176, Ala275. The 9π carbon interaction observed at Asp175.

Journal of Chemical and Pharmaceutical Sciences -JCHPS (2025) 18 (3): 24-32
Online ISSN: Online 2349-8552, Print ISSN: 0974-2115
Research Article | Pharmaceutical Sciences | MCI Approved | Peer-Reviewed | Referred | OA Journal |

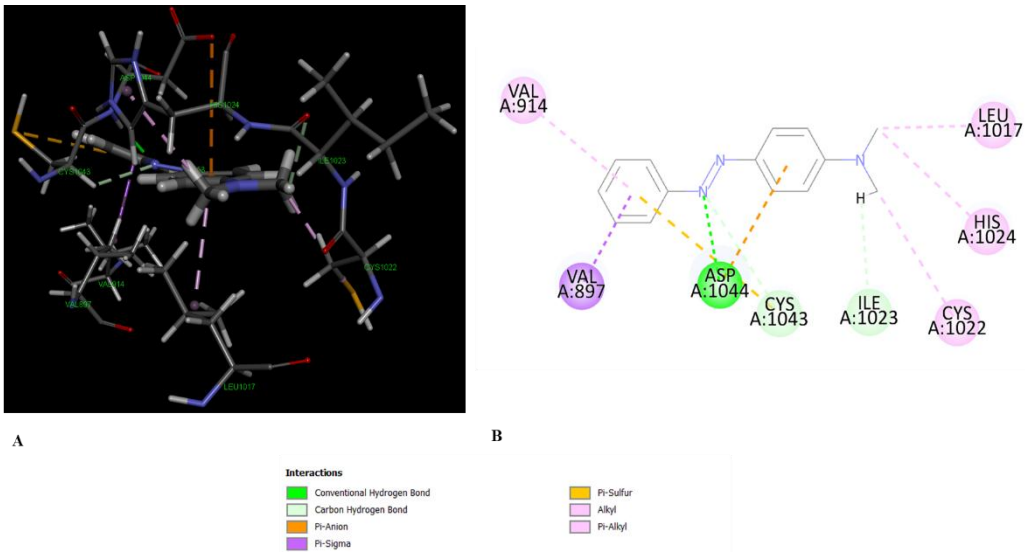

Figure 7: Anticancer activity of DMY with 2oh4 amino acid residues. DMY interacted with **2oh4 protein amino acid residues**-conventional hydrogen band seen at Asp1044, C-H band interaction noted at Cys1043 and Ile1023, while the π- alkyl interaction observed at Val914, Leu1017, His1024, Cys1022.

Molecular docking of DMY is illustrated in Figures 6 and 7. These figures depict the 2D and 3D interactions of the EGFR complex with EREG (PDB ID: 5WB7) with DMY. The target proteins amino acid interactions with DMY (ID No. 6053) are detailed below. **1r51 amino protein**: Two C-H interactions were observed in alkyl at Arg176 and Ala275. A ππ carbon interaction was observed at Asp175. The Lib Dock score is 73.78. **2oh4 amino protein**: A conventional hydrogen band was seen at Asp1044, C-H band interactions were noted at Cys1043 and Ile1023, while ππ -alkyl interactions were observed at Val914, Leu1017, His1024, and Cys1022. The Lib Dock score is 81.48.

The anticancer activity parameters of DMY, as determined by the AutoDock method, are as follows:

- **ADMET Solubility Level**: Approximately 2, indicating moderate solubility. ADMET refers to Absorption, Distribution, Metabolism, Excretion, and Toxicity—key pharmacokinetic processes that describe how a compound is absorbed, processed, and eliminated by the body.
- **ADMET Blood-Brain Barrier (BBB) Level**: Approximately 0, suggesting that DMY is unlikely to penetrate the central nervous system via the BBB.
- **ADMET EXT Hepatotoxic Applicability**: The model descriptor (MD) value is 45998. Drug-induced hepatotoxicity refers to liver damage caused by pharmaceutical or herbal compounds and remains a diagnostic challenge.
- **ADMET EXT CYP2D6 Inhibition Prediction**: False, indicating that DMY is not predicted to inhibit the cytochrome P450 2D6 enzyme.
- **ADMET EXT Hepatotoxicity Prediction**: True, suggesting a potential risk of liver toxicity.
- **ADMET EXT Plasma Protein Binding (PPB) Prediction**: True, indicating that DMY is likely to bind significantly to plasma proteins.

Plasma protein binding (PPB) for siRNA measures the unbound fraction (fu) of the molecule in the plasma at equilibrium. This parameter is crucial in drug development, as regulatory filings for small molecules typically require PPB data. According to the free drug hypothesis, the unbound fraction in plasma reflects the drug concentration available at the site of action under steady-state conditions.

4. CONCLUSION

DMY exhibited a single emission in different solvents, α-CD and β-CD. Compared to water, a red and broad shifted emission observed in the CD solutions. The horizontal band length of DMY was found to be higher than the cavities of α-CD and β-CD, suggesting that the molecule is partially entrapped within the CD cavity. The HOMO-LUMO gap for the DMY/β-CD was more negative, indicating that this is firmer than the DMY/α-CD. Further, compared to the DMY/CD, the red or blue shifts were observed in the absorption and fluorescence in the ZnO/DMY/β-CD nanocomposites. TEM images revealing the formation of nanocrystals in the ZnO/DMY/β-CD composite. The anticancer activity was assessed through molecular docking studies, which indicated that DMY was interacted with **1r51 and 2oh4 amino proteins**.

ACKNOWLEDGEMENT

This work was supported by the Rashtriya Uchchatar Shiksha Abhiyan (RUSA) Phase -2.0 [No. 128/A1/ RUSA 2.0, Health and Environment] New Delhi, India.

REFERENCES

[1] Rasmussen, J.W., Martinez, E., Louka, P., Wingett, D.G. Zinc oxide nanoparticles for selective destruction of tumor cells and potential for drug delivery applications. Expert Opinion on Drug Delivery, 2010; 7:1063–1077. DOI: 10.1517/17425247.2010.502560
[2] Xiong, H.M. ZnO nanoparticles applied to bioimaging and drug delivery. Advanced Materials, 2013; 25: 5329–5335. doi.org/10.1002/adma.201301732
[3] Sharma, H., Kumar, K., Choudhary, C., Mishra, P.K., Vaidya, B. Development and characterization of metal oxide nanoparticles for the delivery of anticancer drug. Artificial Cells, Nanomedicine, and Biotechnology, 2016; 44:672–679. DOI: 10.3109/21691401.2014.978980
[4] Zhang, Y., Nayak, T.R., Hong, H., Cai, W. Biomedical applications of zinc oxide nanomaterials. Current Molecular Medicine, 2013; 13:1633–1645. doi: 10.2174/15665240136661311111300 58.
[5] Martinez-Carmona, M., Gun'ko, Y., Vallet-Regi, M. ZnO nanostructures for drug delivery and theranostic applications. Nanomaterials, 2018; 8:268. doi.org/10.3390/nano8040268
[6] Bettini, S, Pagano, R, Bonfrate, V, et al., Promising piezoelectric properties of new ZnO@octadecylamine adduct. J Phy Chem C, 2015; 119: 20143–20149. doi.org/10.1021/acs.jpcc.5b06013
[7] Pagano, R., Quarta, A., Pal, S., Licciulli, A., Valli, L., Bettini, S. Enhanced solar-driven applications of ZnO@Ag patchy nanoparticles. J Phy Chem C, 2017; 121: 27199–27206. doi.org/10.1021/acs.jpcc.7b09594.
[8] Bettini, S., Pagano, R., Valli, L., Giancane, G. Enhancement of open circuit voltage of a ZnO-based dye sensitized solar cell by means of piezotronic effect. Chemistry-An Asian Journal, 2016; 11: 1240–1245. doi.org/10.1002/asia.201501325
[9] Jinhuan Jiang, Jiang Pi, Jiye Cai, The Advancing of Zinc Oxide nanoparticles for Biomedical Applications, Bioinorganic Chemistry and Applications (Hindawi), Article ID 1062562, 2018; 1-18. doi.org/10.1155/2018/1062562
[10] Ramasamy, P., Mani, A., Sneha, B., Nivetha, E., Venkatesan, M., Rajendiran, N. Azo-hydrazo tautomerism in Sudan Red-B and Cyclodextrin/Sudan Red-B doped ZnO nanomaterials. J. Mol. Struc., 2025; 1329: 141423-431. doi.org/10.1016/j.molstruc.2025.141423
[11] Mani, A., Ramasamy, P., Antony Muthu Prabhu, A., Rajendiran, N. Investigation of Ag and Ag/Co bimetallic nanoparticles with naproxen-cyclodextrin inclusion complex**.** J.Molecular Structure 2023; 1284: 135301-10, doi.org/10.1016/j.molstruc.2023.135301
[12] Mani, A., Venkatesh, G., Senthilraja, P., Rajendiran, N. Synthesis and Characterisation of Ag-Co-Venlafaxine-Cyclodextrin Nanorods. European J Advanced Chemistry Research, 2024; 5: 9-16. doi; 10.24018/ejchem.2024.5.1.147
[13] Mani, A., Ramasamy, P., Antony Muthu Prabhu, A., Senthilraja, P., Rajendiran, N. Synthesis and Analysis of Ag/Olanzapine /Cyclodextrin and Ag/Co/Olanzapine /Cyclodextrin Inclusion Complex Nanorods. Physics and Chem. Liquids, 2024; 62: 196-209. doi.org/10.1080/00319104.2023.2297223
[14] Mani, A., Ramasamy, P., Antony Muthu Prabhu A., Senthilraja P., Rajendiran, N. Synthesis and Characterisation of Ag/Co/Chloroquine/Cyclodextrin Inclusion Complex Nanomaterials *J* Sol-Gel Science and Technology, in press 2005; doi.org/10.1007/s10971-024-06620-5.

[15] Morris, G.M., Goodsell, D.S., Halliday, R.S., Huey, R., Hart, WE., Belew, RK., Olson, AJ. Automated docking using a Lamarckian genetic algorithm and an empirical binding free energy function. J Comput Chem. 1998; 19(14): 1639–1662. https://doi.org/10.1002/(SICI)1096-987X(19981115)19:14<1639::AID-JCC10>3.0.CO;2-B
[16] Huey, R., Morris, G.M., Olson, A.J., Goodsell, D.S. A semiempirical free energy force field with charge-based desolvation. J Comput Chem. 2007; 28(6): 1145–1152. DOI: 10.1002/jcc.20634
[17] Morris, G.M., Lim-Wilby, M. Molecular docking In: Kukol A (ed) Molecular modeling of proteins, Methods in molecular biology, Humana, Totowa, N J. 2008; 443: 365–382. DOI: 10.1007/978-1-59745-177-2_19
[18] Trott, O., Olson, A.J. AutoDock Vina: improving the speed and accuracy of docking with a new scoring function, efficient optimization, and multithreading. J Comput Chem, 2010; 31(2): 455–461. DOI: 10.1002/jcc.21334
[19] Anthony D Hill, Peter J Reilly. Scoring Functions for AutoDock, Methods in Molecular Biology, Springer, 2015; 1273: 467-474. DOI: 10.1007/978-1-4939-2343-4_27
[20] Halgren, T A. Merck Molecular Force Field. I. Basis, Form, Scope, Parameterization, and Performance of MMFF94. J Comput Chem. 1998; 17: 490-519. doi.org/10.1002/(SICI)1096-987X(199604)17:5/6<490::AID-JCC1>3.0.CO;2-P.
[21] Roskoski, Jr R. The ErbB/HER family of protein-tyrosine kinases and cancer. Pharmacological Research, 2014; 79: 34-74. DOI: 10.1016/j.phrs.2013.11.002
[22] Sunaga, N., Kaira, K. Epiregulin as a therapeutic target in non-small-cell lung cancer. Lung Cancer: Targets and Therapy, 2015; 12(6): 91-98. DOI: 10.2147/LCTT.S60427
[23] Antony Muthu Prabhu, A., Venkatesh, G., Sankaranarayanan, RK., Rajendiran, N. Azonium-ammonium tautomerism and inclusion complexation of 4-amino-2', 3-dimethyl azobenzene. Indian J Chem. 2010; 49A: 407–417.
[24] Venkatesh, G., Sankaranarayanan, R.K., Antony Muthu Prabhu, A., Rajendiran, N. Azonium-Ammonium Tautomerism and Inclusion Complexation of 1-(2,4-diamino phenylazo) naphthalene and 4-Amino azobenzene. J Fluores. 2011; 21: 1485-1497. doi.org/10.1007/s10895-011-0835-1
[24] Venkatesh, G., Saravanan, J., Rajendiran, N. Cyclodextrin covered organic micro rod and micro sheet derived from supramolecular self-assembly of 2,4-dihydroxy azobenzene and 4-hydroxy azobenzene inclusion complexes. Bull Chem Soc Jpn. 2014; 87: 283-293. doi.org/10.1246/bcsj.20130255
[25] Antony Muthu Prabhu, A., Venkatesh, G., Rajendiran, N. Azo-Hydrazo tautomerism in 1-phenyazo-2-naphthol dyes in various solvents, pH and β-CD. J Fluores 2010; 20: 961–972. doi.org/10.1007/s10895-010-0642-0.
[26] Prema Kumari, J., Antony Muthu Prabhu, A., Venkatesh, G., Subramanian, V.K., Rajendiran, N. Effect of solvents and pH on β-CD Inclusion complexation of 2,4-dihydroxy azobenzene and 4-hydroxy azobenzene. J Solution Chem. 2011; 40: 327–347. doi.org/10.1007/s10953-010-9639-1.
[27] Rajendiran, N., Sankaranarayanan, R.K. Azo dye/Cyclodextrin: New findings of identical nanorods through 2:2 inclusion complexes. Carbohydrate Polymers 2014; 106: 422-431. doi.org/10.1016/j.carbpol.2014.01.030.
[28] Rajendiran, N., Venkatesh, G., Saravanan, J. Encapsulation of thiazoresorcinol and thiazocresol dye within α- and β-CD cavities: Spectral and molecular modeling studies. J Mol Struc. 2014; 1072: 242-252. doi.org/10.1016/j.molstruc.2014.05.018.
[29] Siva, S., Thulasidhasan, J., Rajendiran, N. Host-guest inclusion complexes of propafenone hydrochloride with α- and β-cyclodextrins: Spectral and molecular modeling study. *Spectrochim Acta*, 115A (2013) 559–567. doi.org/10.1016/j.saa.2013.06.079
[30] Venkatesh, G., Sankaranarayanan, R.K., Antony Muthu Prabhu, A., Rajendiran, N. Absorption and fluorescence spectral characteristics of norepinephrine, epinephrine, isoprenaline, methyldopa, terbutaline and orciprenaline drugs. *Physics and Chemistry of Liquids*, 50 (2012) 434-452. doi.org/10.1080/00319104.2011.597029
[31] Rajendiran, N., Balasubramanian, T. Dual fluorescence of syringaldazine. *Spectrochim Acta*, 68A (2007) 894–904. doi.org/10.1016/j.saa.2007.01.004
[32] Antony Muthu Prabhu, A., Sankaranarayanan, R.K., Siva, S., Rajendiran, N. Intra molecular proton transfer effects on 2,6-diaminopyridine. *J. Fluorescence*, 20 (2010) 43–54, doi.org/10.1007/s10895-009-0520-9
[33] Rajendiran, N., Swaminathan, M. Spectral characteristics of 4-aminodiphenyl ether in different solvents and various pH. *J. Photochem. Photobiol. A: Chem.*, 93 (1996) 103-108. doi.org/10.1016/1010-6030(95)04189-3
[34] Stalin, T., Vasantharani, P., Shanthi, B., Sekar, A., Rajendiran, N. Inclusion complex of 1,2,3-trihydroxybenzene with α- and β-cyclodextrins. *Indian J Chemistry*, 45A (2006) 1113–1120.
[35] Sivakumar, K., Stalin, T., Rajendiran, N. Dual fluorescence of diphenyl carbazide and benzanilide: Effect of solvents and pH on electronic spectra. *Spectrochimica Acta*, 62A (2005) 991–999. doi.org/10.1016/j.saa.2005.04.033